

Launch Vibration Damping Using Slip in Pretensioned Coils

Alexander Wen* and Sergio Pellegrino†
California Institute of Technology, Pasadena, CA, 91125

Vibration management is important for the survivability of structures during launch, and is particularly challenging for large deployable space structures. Adding damping to a structure reduces the overall level of response excitation, which increases survivability. Structural damping occurs through the dissipation of energy during vibration. One such energy dissipation mechanism that can be utilized to increase damping is friction, such as the friction between slipping layers of a wound roll. In this paper, we study the vibration response of a structure, which has a pre-tensioned coil wound around it. Here, the damping is provided by friction between slipping layers in the pre-tensioned coil. An experiment is performed on a small-scale setup to evaluate the feasibility of this approach by measuring the frequency response and damping under different winding tensions. The same setup is used to measure layer slip during vibration, using a high speed camera and tracking targets to identify the regions with the largest slip, indicating higher contribution to energy dissipation. To confirm understanding of the damping mechanism, a 3D finite-element simulation is created in an attempt to capture the variation in frequency response and locations of slip with winding tension measured experimentally.

I. Introduction

Vibration management is important for the survivability of structures during launch. There are two primary approaches for vibration mitigation: increasing stiffness or adding damping. In this paper, we study the damping approach, which utilizes energy dissipation to reduce amplitudes of excitation. There have been a variety of passive, mechanical dampers proposed including: tuned mass dampers, liquid sloshing dampers, particle dampers, as well as friction-based dampers [1–5]. However, the concept of *adding* damping, underscores that these types of dampers are not intrinsic to the original structure, and thus their addition results in an increase in mass and complexity of the system.

Motivation for this work looks to state of the art deployable structures for space, where coiling as a packaging architecture has seen increased usage for structures such as IKAROS, ROSA, and Starshade [6–8]. Here, looking at these structures in the stowed, coiled configuration, we ask whether it is possible to make use of the existing mass and re-purpose it as multi-functional, by having the coil itself provide an energy dissipation mechanism for damping. Prior studies indicated that both the stiffness and interlayer slip of a wound roll undergoing vibration can be adjusted by varying the winding tension [9, 10]. Thus, we propose a variant of friction damping using a pre-tensioned, wound roll. In this scheme, the roll is wound around a base structure with a tension that allows some degree of interlayer slip during vibration. The friction between slipping layers provides the energy dissipation mechanism, which provides damping to the system undergoing vibration, thereby reducing the overall level of excitation.

The objective of this research is to investigate how a coiled roll may be used as a passive, vibration damping device, which utilizes friction as the energy dissipation mechanism. To do this, we first experimentally evaluate the effectiveness of this scheme by measuring how the winding tension of the roll during coiling affects the vibration response on a small-scale structural model. This is done by performing modal characterization of a wound roll assembly using a low level sine sweep test. Damping is extracted from the experimental frequency response spectrum by using the half-power bandwidth method on the first peak acceleration response.

Next, we want to identify the locations in the coil that are responsible for the damping energy dissipation mechanism by experimentally measuring layer slip during vibration. This will provide understanding of how the vibration dynamics dictate the active regions within the coil for the wound roll damper concept. The slip measurement experiment is conducted using the same test sample used in the frequency response characterization. To measure slip, reference tracking targets are placed at several locations along the length of the base structure. As a single, continuous membrane is wound around the structure, additional tracking targets are placed on alternating layers, concentric to the base reference

*PhD Candidate, Graduate Aerospace Laboratories, 1200 E. California Blvd, MC105-50, Pasadena. email: awwen@caltech.edu.

†Joyce and Kent Kresa Professor of Aerospace and Professor of Civil Engineering, Graduate Aerospace Laboratories, 1200 E. California Blvd, MC105-50, Pasadena. AIAA Fellow. email: sergiop@caltech.edu.

targets. The wound roll is then excited using a sine dwell test at the natural frequency of the assembly, and a high speed camera captures the position of the tracking targets. Measurements are performed both axially and transverse to the axis of vibration. The high speed camera images are processed by identifying the centroids of the targets, where the difference between the layer target and the reference indicates slip relative to the base structure, and the difference between layer targets indicates interlayer slip.

Following these experiments, a finite-element analysis (FEA) is performed in order to build a model that correlates with the variations in damping and locations of slip observed in the experiments. The simulation is conducted on a simplified, 3D representation of a wound roll, which consists of several concentric, cylindrical shells, which approximate coiled layers around a mandrel. For this simulation, we use geometry and properties derived from the experimental setup. The coil layers are preloaded against the elastic mandrel using a range of pressures, and a friction interaction is defined between all adjacent contact surfaces. Base excitation is then applied, both in the form of sine sweep and sine dwell. The simulation is integrated in time, and the tip and base accelerations are recorded for the sweep excitation, while the contact status of all elements is recorded for the dwell excitation. The simulated frequency response, corresponding damping values, and slip locations are then compared against the experimentally measured values.

II. Vibration Experiment Setup and Procedure

A. Experiment setup

The vibration experiment consists of shaking 25 layers of 2 mil thick Kapton®HN membrane, consisting of one continuous sheet wound around a polycarbonate mandrel via a winding machine. The configuration here is derived from a previous experiment, where the materials and geometry were chosen so that a relatively small amount of layers would have a sizeable impact on the structural response of the system [9]. We note that the stiffness and mass of the constituent materials of the mandrel and membrane are approximately equal. Before the first winding, circular reference tracking targets are applied to the mandrel surface at several locations near the base of the mandrel, Fig. 1a. One end of the membrane is attached to the mandrel using tape, and the membrane is then wound over the initial reference targets. During winding, circular ring targets are placed on subsequent alternating layers, concentric to the reference targets. The tracking targets are placed only along one longitudinal line of the cylindrical sample. After coiling is complete, the free end of the membrane is fixed to the outer surface of the roll with tape, Fig. 1b.

An internal illumination source allows the tracking targets to be visible through the transparent mandrel and membrane layers, Fig. 1c. The internal surface of the mandrel was covered with aluminized Mylar, which creates a mirrored surface that focuses the internal illumination onto a narrow section of the test sample containing the line of targets in order to increase signal strength during high speed camera measurements. The coiled roll was assembled using a range of different winding tensions, and parameterized by the interlayer stress measured at the innermost layer using a pressure sensor. The preloaded, coiled assembly was then placed on a vibration table, and a retro-reflective tracking marker was placed near the tip of the assembled roll on the outer layer as well as on the shaker head as depicted in Fig. 2. The retroreflective tracking markers were used in concert with a Polytec PSV-500 Laser Scanning Vibrometer.

B. Vibration response experiment procedure

The vibrometer was used to control the vibration table in order to first perform a low-level sine sweep for each winding tension case for the damping response characterization experiment. The sweep is run from 5 to 300 Hz for a 45 s duration. The acceleration spectrum of the tip tracking marker and the vibration table shaker head marker are recorded in order to provide an acceleration transmissibility response curve. Damping is estimated from the experimental transmissibility spectrum by using the half-power bandwidth method on the first peak acceleration response, which corresponds to the natural frequency of the wound configuration.

C. Layer slip measurement procedure

Next, a sine dwell at the identified natural frequency is performed for the layer slip measurement experiment. The internal illumination source is turned on, allowing a high speed camera to record the tracking targets during the vibration experiment at 2000 fps. The experiment was performed both for a ‘loosely wound’ case and a ‘tightly wound’ case. The slip measurement for each of the two tension levels tested is performed twice: once with the camera viewing direction aligned axially to the excitation direction and once in the transverse direction, Fig. 2. Because the tracking targets are placed only along one longitudinal line along the test sample, the wound roll and the high speed camera position must

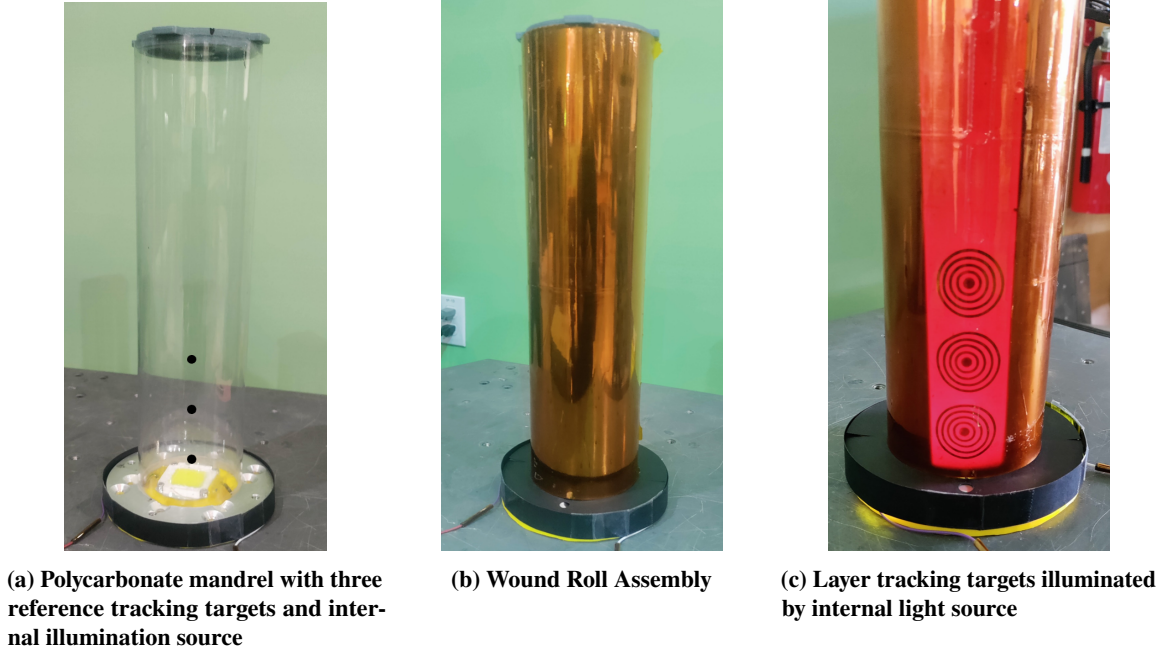


Fig. 1 Wound roll damper test sample.

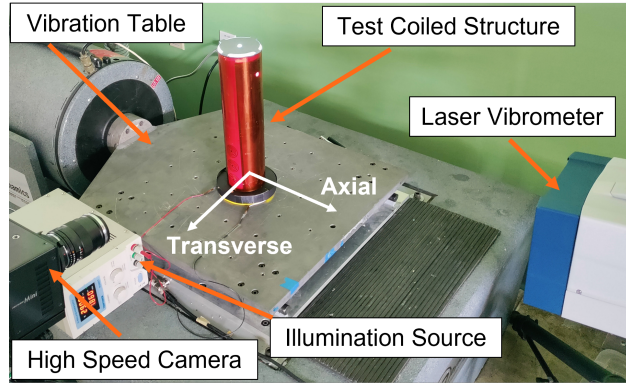


Fig. 2 Vibration experiment on a wound roll.

be rotated for each viewing direction.

Images from the high speed camera were exported onto a personal computer and processed using MATLAB. Each frame was thresholded to create a grayscale image of binary values. The targets in the processed image are identified by the number of connected pixels, as well as their circularity and diameter. Once successfully identified, the centroids of each target, measured in the image coordinate frame, (x, y) , were stored. A centroid based tracking scheme was found to be more robust compared to an edge detection scheme, which was highly sensitive to imaging noise resulting from high frame rate imaging that measured low signal-to-noise due to lower exposure time. Fig. 3 shows an example processed image that indicates the accuracy of the centroid tracking scheme for one particular image. The targets at a given longitudinal position are denoted as Group i . The targets on a given layer are denoted with Layer j . For a given target Group i , subtracting the position of the reference target, $(x_r, y_r)_i$ from the position of the layer targets, $(x, y)_i^j$, eliminates the contribution of the mandrel movement. The resultant is the slip of layer j , $(s_x, s_y)_i^j$, relative to the mandrel:

$$(s_x, s_y)_i^j = (x_r, y_r)_i - (x, y)_i^j \quad (1)$$

Interlayer slip can then be computed by taking the difference between layers:

$$(s_x, s_y)_i^{j_1 - j_2} = (s_x, s_y)_i^{j_1} - (s_x, s_y)_i^{j_2} \quad (2)$$

Note that the slip calculations in Eq. (1) and Eq. (2) are performed in the time domain and the units are in pixels.

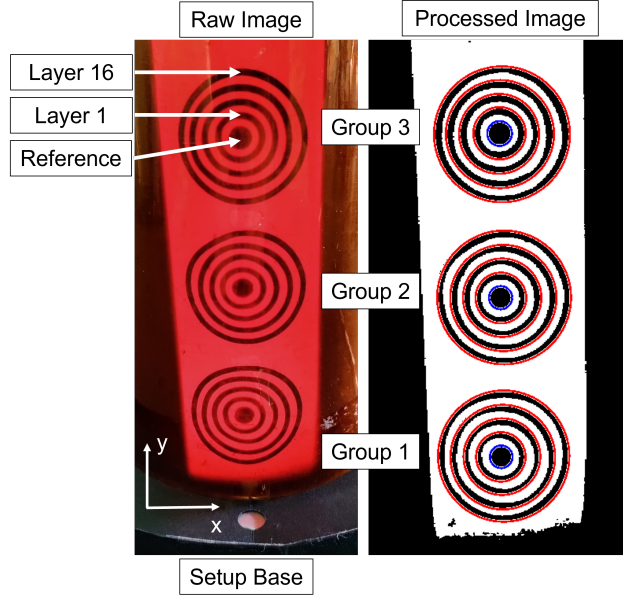


Fig. 3 Example processed image showing centroid tracking scheme. Here, layer targets were placed every five layers starting from Layer 1 (Layers 1, 6, 11, 16).

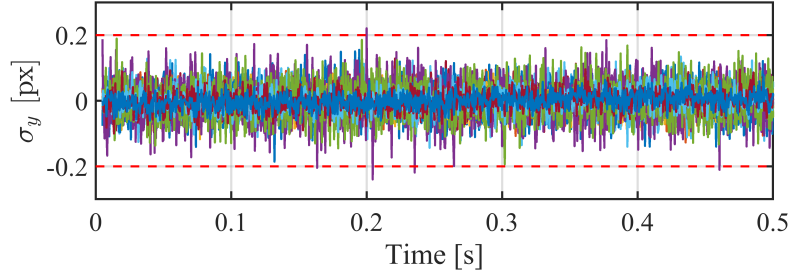
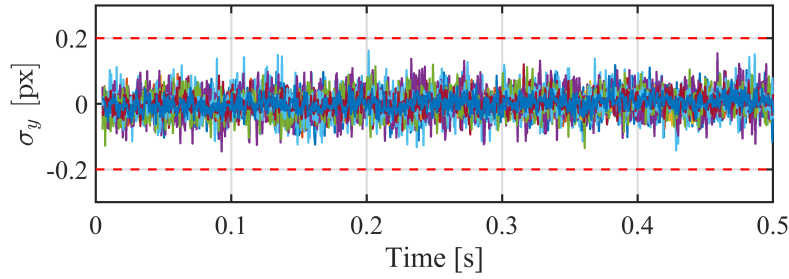
The noise floor of the measurement and processing chain was evaluated by applying the entire procedure to the sample measured at rest. High frequency noise present in the statically measured centroids in the time domain, Fig. 4a, motivated performing analysis in the frequency domain and only considering the frequency range of interest that was tested experimentally, Fig. 4b. This was done by taking the Fourier Transform of the time domain signals, which was a preferred method over directly filtering or smoothing the time domain data to avoid impacting the slip measurement. From this, the maximum uncertainty in the position of the targets measured statically in the frequency band of interest was found to be $\sigma = \max(\sigma_x) = \max(\sigma_y) \approx 0.01$ px. Since we calculate the slip from the difference of two uncertain measurements, the propagation of uncertainty results in a total slip noise floor of $\sigma_s = \sqrt{2}\sigma \approx 0.02$ px. Slip magnitudes at least σ_s above the noise floor would be considered as a real signal, whereas values below this threshold would be considered indistinguishable from the static, no slip condition. As a result, after first performing slip calculations in the time domain, the results are converted into the frequency domain for evaluation.

III. Vibration Experiment Results

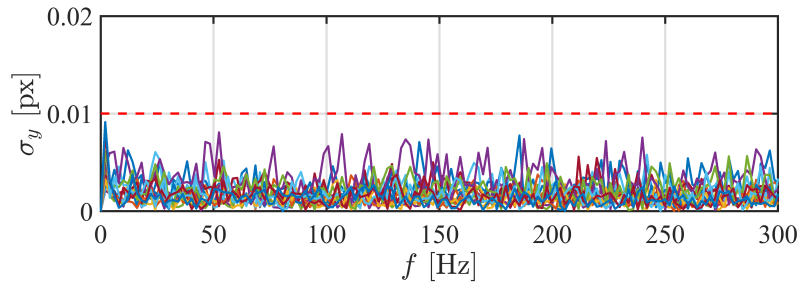
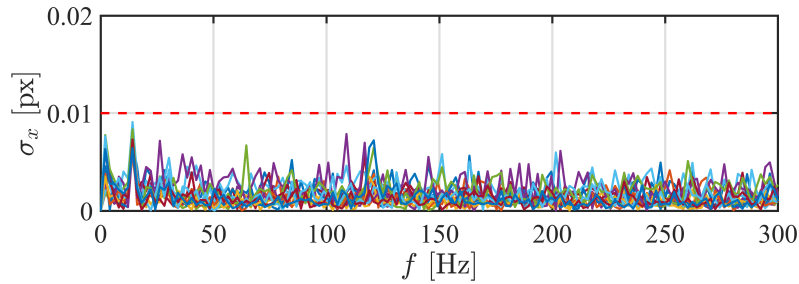
A. Vibration response of wound roll damper with winding tension

The frequency responses of the wound roll with different winding tensions were measured and are shown in Fig. 5a. From these curves, we extract the natural frequency, f_n and estimate the damping, ξ_{est} . The damping of the wound roll, plotted against the measured natural frequency of the wound roll normalized against the natural frequency of the mandrel measured by itself, is shown in Fig. 5b. The response and damping of the mandrel by itself is also shown in these figures.

From these plots, we observe an apparent bimodal response between ‘loosely wound’ and ‘tightly wound’ cases for the range of winding tensions studied. We note there is some variability in distinguishing responses by the winding pressures, likely due to the single point measurement of winding stress being of insufficient repeatability. This can be mitigated in future experiments by taking the average of multiple measurements using multiple flexible pressure sensors simultaneously. Despite this limitation, the difference in stiffness, amplitude of response, and damping are large enough that there is a clear delineation between ‘loosely wound’ and ‘tightly wound’.



(a) Time domain centroid locations of all 15 targets measured statically.

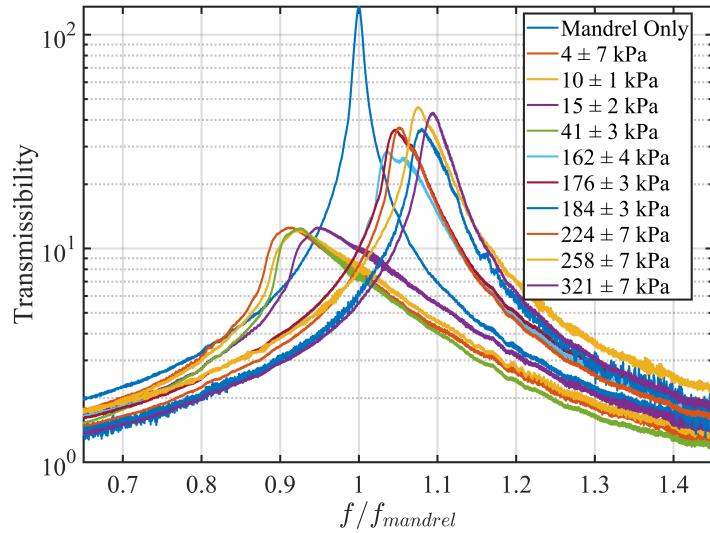


(b) Frequency domain centroid locations in frequency band of interest of all 15 targets measured statically.

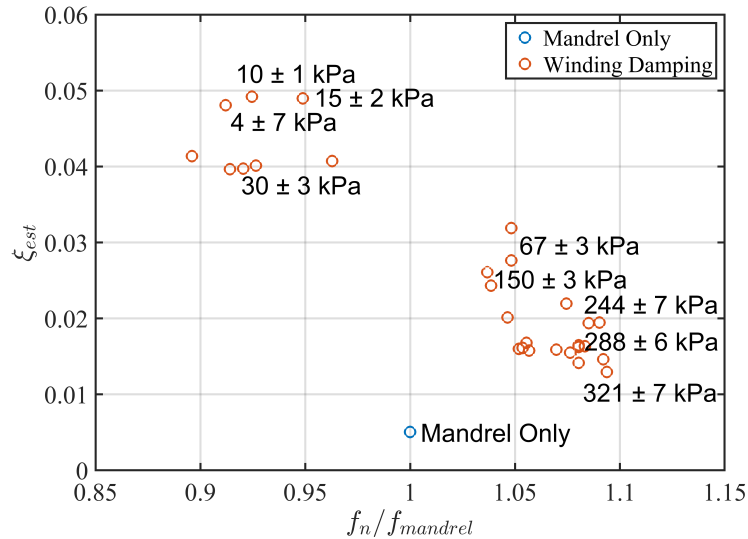
Fig. 4 Noise floor estimation of measurement and centroid tracking processing chain.

For loosely wound setups, we observe that the assembly exhibits reduced stiffness and significantly increased damping relative to the response of the mandrel by itself. Conversely, the tightly wound cases demonstrate increased stiffness and comparatively less damping than the loosely wound cases. However, regardless of the winding tension, we observe that the addition of the wound roll has increased the overall damping of the assembly. The estimated range of critical damping varies from 1 - 5%, increased over the ‘mandrel-only’ result of approximately 0.5%. The penalty in reduced stiffness in exchange for increased in damping observed in the loosely wound case is seen to be comparatively small for this assembly, as the observed natural frequency was reduced by only approximately 10%. For tightly wound

cases, the clustering of values across a comparatively wide range of winding tensions suggests there may be a saturating level of winding tension, beyond which there is little additional effect in reducing slip for this level of excitation. An approximately 5 - 10% increase in stiffness was observed for tight winding while still maintaining increased damping over the ‘mandrel-only’ case. In general, we see that increasing the winding tension from a loosely wound state results in an overall increased stiffness, but corresponds with decreasing damping. These results confirm the potential of the wound roll damping concept, which utilizes the wound roll as an energy dissipation mechanism.



(a) Transmissibility response spectrum



(b) Damping variation with winding tension

Fig. 5 Wound roll damper frequency response and damping variation.

B. Layer slip measurement

Having now examined the vibration response and performance of the wound roll damper, we are interested in experimentally confirming the underlying mechanism for energy dissipation is, in fact, layer slip. Therefore, we want to correlate increased winding tension with reduced layer slip and identify locations that have the largest amount of slip.

Knowledge of slip magnitude by layer and location will provide insight into how the vibration dynamics dictate what layers and positions are active in the wound roll damping scheme.

First, we make an aggregate slip plot, which plots the maximum, mandrel relative slip, in any direction (x, y) at any layer, $\max_j[(s_x, s_y)_i^j]$, against the target groupings for both axial and transverse measurements, Fig. 6. In this figure, the error bar corresponds to the uncertainty of the measurement, σ_s . In examining the data, we observed that slip,

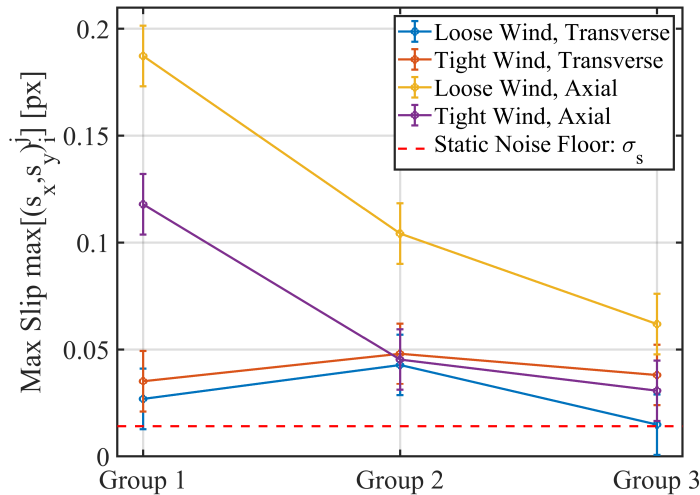


Fig. 6 Aggregate mandrel relative slip: maximum of vertical and horizontal slip at any layer for axial and transverse measurements.

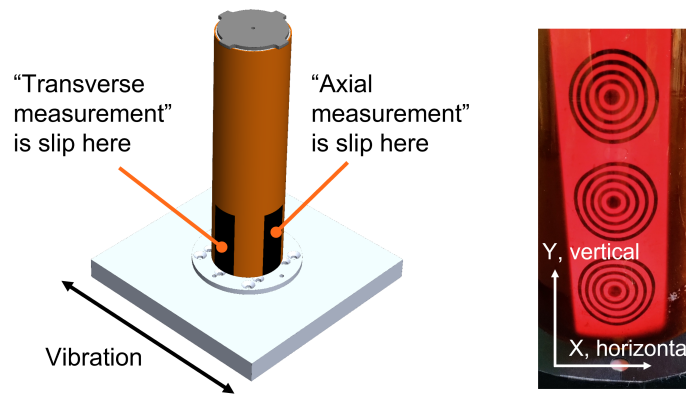
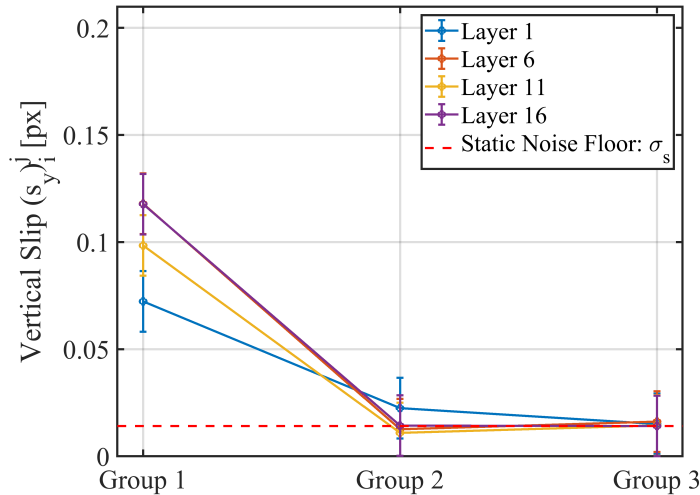


Fig. 7 Slip measurement location and direction conventions.

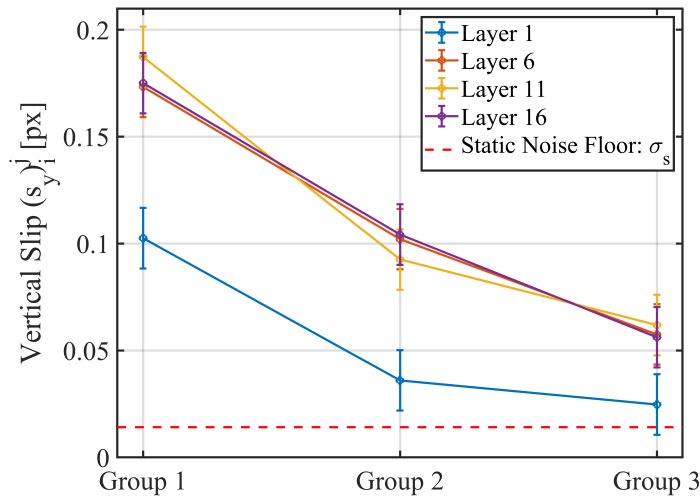
relative to the mandrel, in the transverse direction is much smaller than in the axial direction of measurement, i.e., in the excitation direction, Fig. 7. In the transverse direction of measurement, we see no clear difference between the loose and tight winding: the curves coincide within the uncertainty of the measurement. In the axial direction, there is an unambiguous delineation between tight winding and loose winding, as seen in the difference of the slip magnitudes. Therefore, we can focus our attention on the axial measurements and look at the components of mandrel relative slip, (s_x, s_y) , separately.

In the axial direction, the vertical slip, s_y , is larger than the horizontal slip, s_x , in general, Fig. 7. Thus, we only report the vertical slip data for the axial measurement direction, Fig. 8. Comparing Fig. 8a and Fig. 8b, we again see that

the loosely wound case slips more than the tightly wound case. Maximum slip, in either case, occurs towards the base of structure (Group 1) and falls off further away from the base. Comparing the magnitude of slip by layer, Layer 1 has the lowest slip. But we note that the leading edge of the 1st layer was fixed to the mandrel at the beginning of winding.



(a) Vertical slip by layer and group for tight winding



(b) Vertical slip by layer and group for loose winding

Fig. 8 Comparison between axially measured, vertical slip (s_y) for tight and loose winding.

Examining Fig. 8b, we see that the mandrel relative slip magnitude curves for Layers 6, 11, and 16 coincide. This suggests that after a certain layer, between Layer 1 and Layer 6, there is no more relative movement between layers. This fact is clearly evident when considering the interlayer slip, $(s_x, s_y)_i^{j_1-j_2}$, instead of the mandrel relative slip, as shown in Fig. 9. This figure was obtained by subtracting the centroid position of Layer 6 from the centroid positions of all subsequent layers in the time domain, and then taking the Fourier Transform. Fig. 9 demonstrates that the measured slip relative to Layer 6 is indistinguishable from the static noise floor, which indicates that there is no appreciable interlayer slip beyond Layer 6. This result is consistent with the findings in [9], which indicated that the largest shear stress components for a cylindrical structure, with coordinate frame (R, θ, Z) , undergoing base excitation were the τ_{RZ} shear stresses in axis to the excitation direction. The location of these stresses was at the base of the structure, propagating only a small radial distance away from the innermost layer. From this experiment, we can conclude that due to the

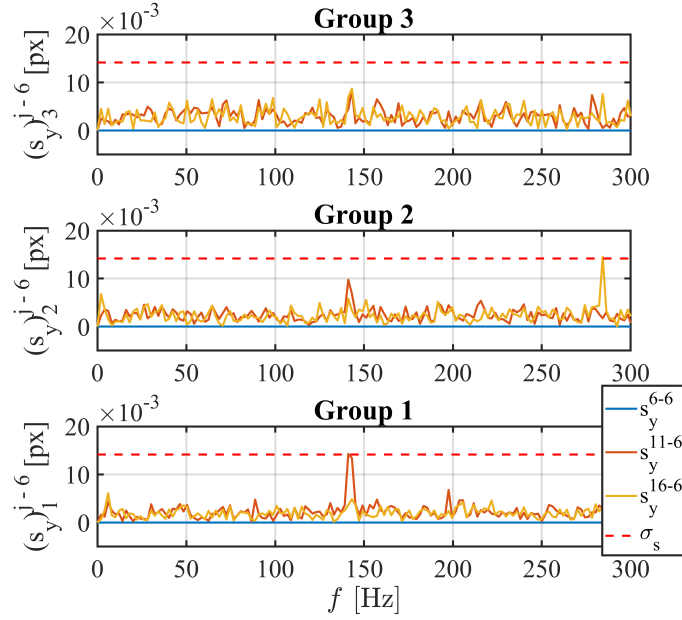


Fig. 9 Interlayer slip for axially measured, vertical slip (s_y) for loose winding.

bending vibration mode of our structure, the inner layers towards the bottom of the roll, in axis of vibration, have the largest effect on dissipation for the wound roll damper concept due to slipping in the vertical direction.

IV. Finite Element Simulation of Wound Roll Damping

The experiments provided evidence for the potential of the wound roll damper as an effective vibration damping scheme. We are now interested in creating a simulation model for analytical and design purposes. The objective of this model is to capture the experimentally observed behaviors:

- 1) Damping and stiffness response with winding tension;
- 2) Inner layers towards bottom of roll, in axis of vibration contribute strongly to the energy dissipation due to slipping in the vertical direction.

An initial attempt was performed by creating a simple FEA model of our experiment setup to determine whether these observed behaviors can be corroborated. Even a qualitative agreement between experiments and simulation would provide a starting point for demonstrating understanding of the key parameters for this frictional damping mechanism.

A. FEA model setup and simulation procedure

The simulation is conducted on a simplified 3D representation of a wound roll that consists of several concentric, cylindrical shells, which approximates coiled layers around a mandrel. Similar to the experiment, we consider the configuration where the coiled structure is supported by an isotropic mandrel, fixed in a cantilevered configuration with a tip mass, m . The coiled structure is represented by n elastic layers placed around the mandrel, with each individual layer preloaded with a pressure loading P . The mandrel is defined by the length L , diameter D , and wall thickness, t_m . The coiled structure is defined by its length L and layer thickness t_l , which is scaled to have total thickness of n layers equivalent to the 25 layers in the experiment, Fig. 10.

For this simulation, we used geometry and properties derived from the experimental setup in Section II.A. The coil layers were preloaded against the elastic mandrel using a range of pressures, and a friction interaction was defined between all adjacent contact surfaces. The contact interface between the coil and mandrel was defined by a Coulomb-like, penalty friction model, with coefficient of friction μ , hard contact, i.e., no penetration, and separation allowed. No other form of damping was included. The mandrel was modeled using S4R shell elements and the coil layers were modeled with M3D4R membrane elements, which have no bending stiffness. The base of the coil was assumed to be bonded to the mandrel's base, Fig. 10.

The properties of the mandrel-coil system are shown in Table 1. These values were determined from a combination of datasheet properties, direct measurement, and correlation from indirect measurements and were adjusted so that the first frequencies of the ‘mandrel-only’ and the mandrel with bonded layers (i.e., no slip), obtained from an eigenvalue frequency analysis, matched experimental values of the corresponding ‘mandrel-only’ and highest preload test cases. In this manner, both the original underlying stiffness of the mandrel by itself and the limiting behavior of no slipping layers were captured.

The finite element software ABAQUS was used to determine the variation in the vibration response of the coil-mandrel assembly, as well as the locations of slip. First, a static analysis was performed to apply the initial preload of the coil layer(s) against the mandrel. In the next dynamics implicit step, the assembly was subjected to one of two acceleration base excitations for each study and time integration of the model response was carried out.

For the frequency response study, sinusoidal base excitation using a geometric chirp base acceleration excitation was applied. Fully modelling 25 layers for the experimental frequency sweep profile and duration was found to be computationally expensive. Therefore, using the results of Section III.B, which indicated that the innermost layers are most significant for damping, we took $n = 1$ layer, and sweep over a reduced frequency range from 125 to 175 Hz at a constant 1 m/s^2 amplitude with a 2 oct/min sweep rate. The output of the sweep simulation reports the time history of the tip response of the coil-mandrel system, as well as the base input. The Fourier Transform of the tip response and base input, and subsequent ratio between the two provides the transmissibility response spectrum in the frequency domain, where the damping is estimated, again, using the half-power bandwidth method.

For the layer slip study, a sine dwell base excitation was prescribed at the original ‘mandrel-only’ frequency, $f_n \approx 155$ Hz. Here, we take $n = 5$ layers in order to determine how many layers does slip propagate through during the vibration event, and run for sufficiently long to reach steady state. Each layer was individually preloaded with preload $P = 200$ Pa. Thus, the total preload on the innermost layer, against the mandrel interface, was 1 kPa. The contact status of the elements for all layers as well as the mandrel was recorded for the dwell excitation, with acceleration amplitudes ranging from $1g - 3g$. The simulated frequency response, corresponding damping values, and slip locations from these two studies can be compared against the experimentally measured values.

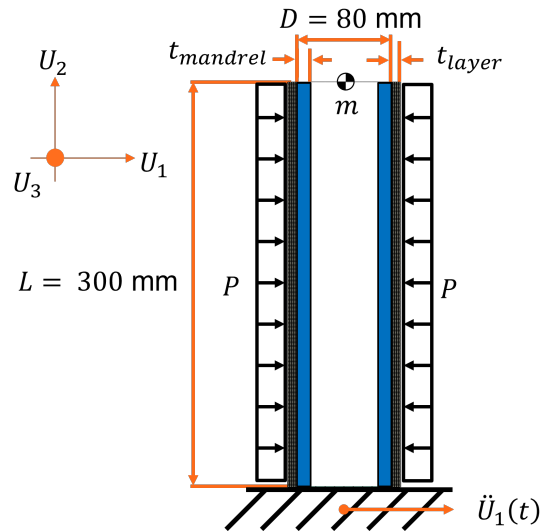


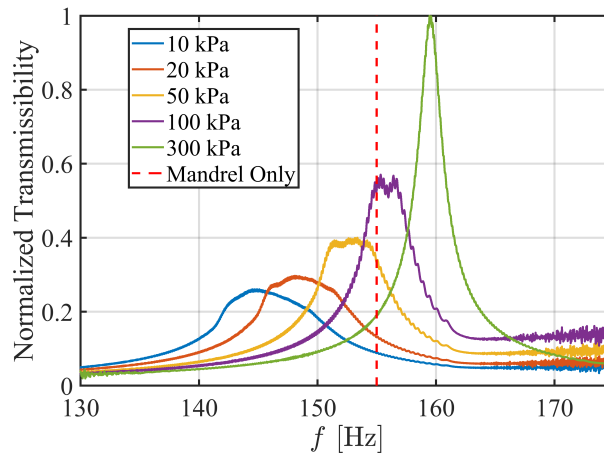
Fig. 10 Geometry of coiled structure for FEA.

Table 1 FEA Model Properties

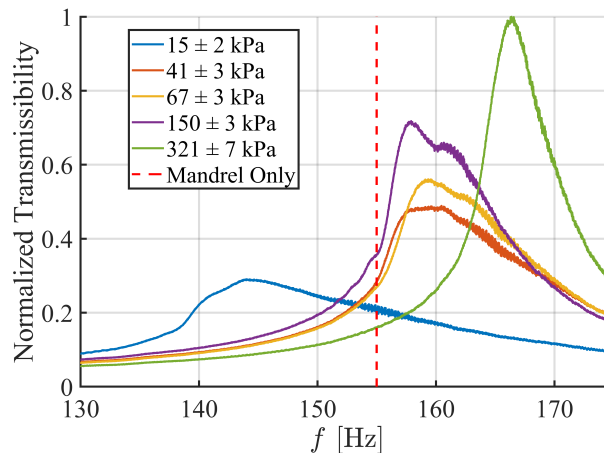
E_m (GPa)	ρ_m (kg/m^3)	E_l (GPa)	ρ_l (kg/m^3)	m (kg)	L (mm)	D (mm)	t_m (mm)	t_l (mm)	n	μ
2.7	1200	2.8	2000	0.05	300	80	1.5	$\frac{25}{n}$ 0.05	1 - 5	0.25

B. Results of frequency response study

A comparison between the simulated frequency responses for a variety of preloads is compared against a set of experimentally measured frequency responses with the closest equivalent measured preloads, Fig. 11. In these plots, the responses are normalized against the peak magnitude of their respective datasets. We observe that there is good, qualitative agreement between our simplified FEA model and our experimental results. The response amplitude in both datasets decreases with decreasing preload, indicating that the looser windings exhibit increased energy dissipation and hence damping. For low preload cases, experimentally we see the frequency response curves are skewed left, which is likewise captured by our FEA model. This behavior is an indication of nonlinear damping or stiffness (softening) [11]. Intermediate preload responses in both simulation and experiment have multiple distinct peaks, suggesting the layer damping scheme is a multi-degree of freedom system, which is characteristic of tuned mass dampers [12]. In addition, we observe that high preload cases converge to a single response peak in both cases, indicating that there is a critical preload for a given excitation level, beyond which slip is significantly reduced and the layer degrees of freedom are eliminated. The reduction in slip with higher preloads results in decreased energy dissipation, causing the excitation response to increase compared to the lower winding tension cases. For both simulation and experiments, the reduction in slip further causes an increase in stiffness relative to the mandrel only response of $f_n \approx 155$ Hz, as seen with the highest preload responses. This indicates that the FEA model successfully captures the stiffening effect where, for sufficiently high pretension, slip is suppressed, and the coiling form factor increases the effective wall thickness of the cylindrical sample, which causes the stiffer response observed.



(a) Abaqus frequency responses



(b) Select experimental frequency responses

Fig. 11 Comparison between simulated and experimentally measured frequency responses.

However, we find there is quantitative disagreement between our simulation and experiments. While, we note that the magnitude of the base excitation in the experiment is larger than that simulated (5 m/s^2 vs. 1 m/s^2), the differences observed are not ameliorated by increasing the simulation excitation level. The simulated response at 1 m/s^2 is softer than the experimental response at 5 m/s^2 , with higher response amplitude. We note that the results of the simulation are sensitive to the interaction between excitation magnitude and the friction capacity, which is the product of the preload and coefficient of friction, as well as the number of layers in the simulation and stiffnesses of the constituent materials. Achieving closer matching between experiment and simulated magnitudes requires understanding of how these parameters interact and is a topic of future study.

Despite the differences between our simulation parameters and experiments, there is a clear similar trend in damping vs. preload, where lower preloads result in increased damping and sufficiently high preloads can result in increased overall stiffness. This is evident when extracting the estimated damping from the simulated responses, Fig. 12. Both datasets exhibit a similar trend line between estimated damping and apparent stiffness. Furthermore, we also note that the estimated damping from simulation has relatively good agreement with the experimentally observed range. While there are discrepancies that result in quantitative inaccuracy, many qualitative behaviors are in agreement between experiments and our FEA model. This suggests that the underlying physics, namely the frictional slip damping and structure dynamic loading interaction, has been captured by our simplified model.

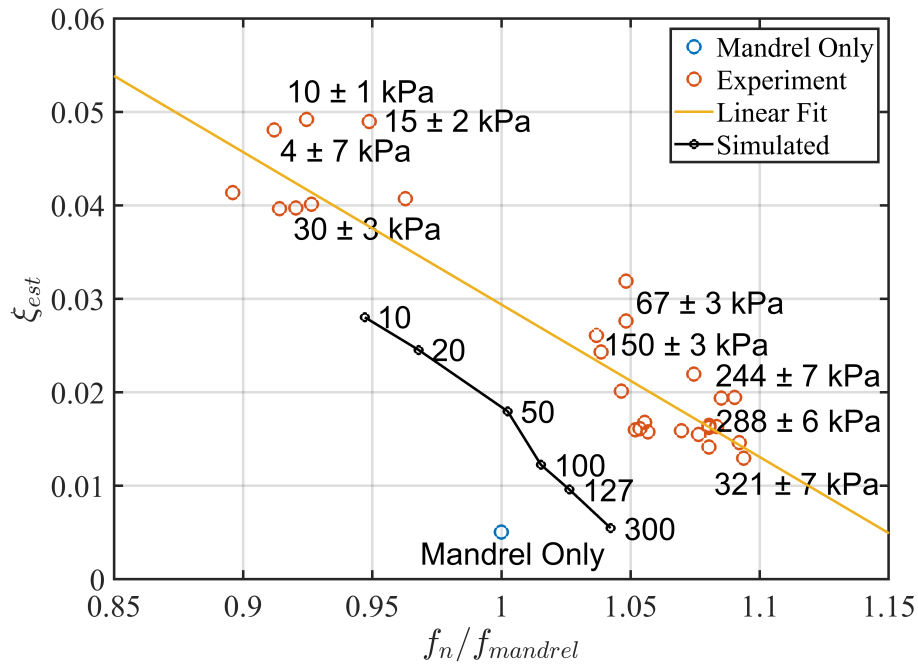


Fig. 12 Damping comparison between simulation and experiment.

C. Results of interlayer slip study

After obtaining qualitative agreement between the simplified FEA model and frequency response experiments, we can reuse this model to determine the locations of slip. Here, the number of layers is increased from the previous study from $n = 1$ to $n = 5$ in order to find where slip occurs and its propagation through the layers. This was done by tracking the contact status of all surfaces, which tracks slipping and sticking contact states. Fig. 13 depicts the cumulative, steady state contact status for each layer across multiple loading amplitudes. Here, ‘cumulative’ meaning these plots depict locations of slip on each layer that was observed at any point during the simulation in red, whereas green denotes sticking, i.e., no slip, observed throughout the entire simulation. In this representation, the slip status of Layer i indicates slip with respect to Layer $i + 1$. From these plots, we again see good, qualitative agreement with the experimental results.

From Fig. 13a, we observe the following behaviors. First, the largest slip area occurs at the innermost interface, between the mandrel and Layer 1. Next, this largest patch of slip is vertical slip that occurs on the faces aligned with

the U1 axis, which is the excitation axis. This can be seen in Fig. 14, which is a vector plot of the maximum, relative displacements between Layer j_1 and the preceding Layer $j_2 = j_1 - 1$, which we denote as $\vec{U}^{j_1-j_2}$. And finally, after a certain layer, no slip is observed on any subsequent outer layers as seen in both Fig. 13a and Fig. 14. All these behaviors are consistent with the findings of the slip measurement experiment. Keeping the friction and preload consistent, increasing the excitation level causes the area of cumulative slip to grow in the vertical direction as well as propagate through additional layers, Fig. 13b and Fig. 13c. This indicates that larger excitations increase the extent of the layers that actively participate in energy dissipation, suggesting that the performance of the wound roll damper inherently scales with the excitation level.

The results of this study demonstrate that the simulation successfully captures the experimentally observed behaviors: the inner layers towards the bottom of the roll, in the axis of vibration, have the largest effect on dissipation for the wound roll damper concept due to slipping in the vertical direction.

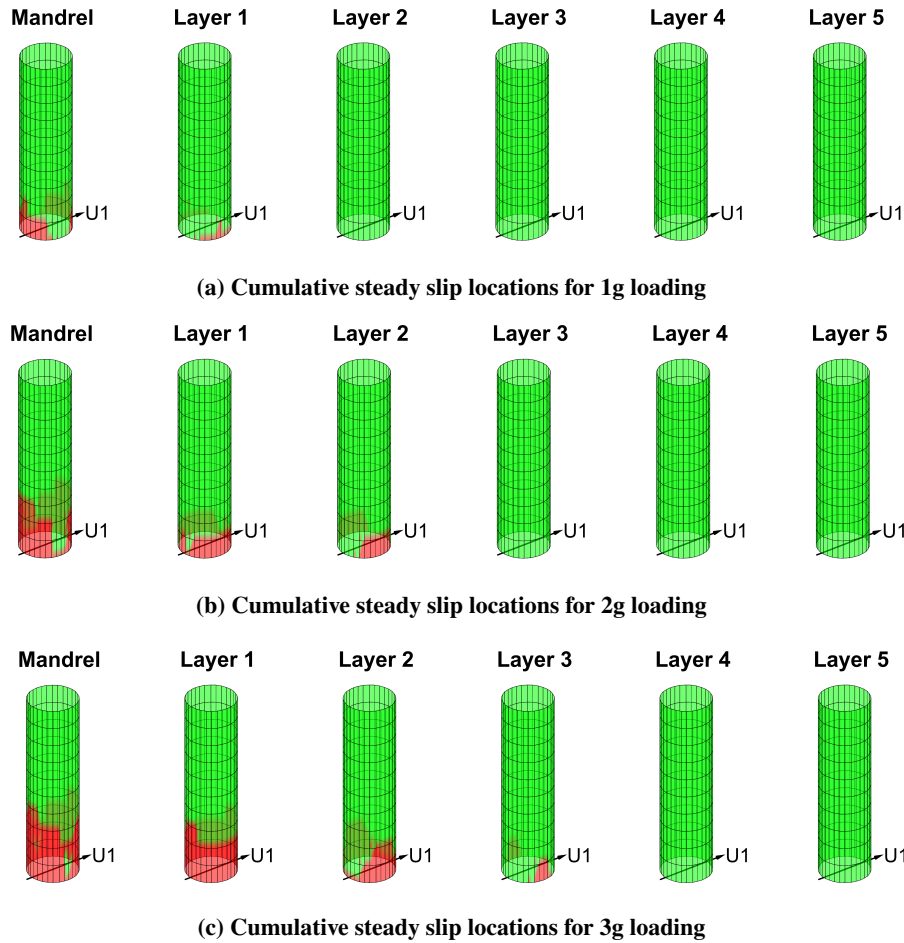


Fig. 13 Locations of slip with loading variation.

V. Conclusion and Future Work

In this study, we have proposed a variant of the friction damper concept, which utilizes interlayer slip of a roll wound around a structure to provide an energy dissipation mechanism to reduce the amplitude of vibration. The performance of the wound roll damper concept was demonstrated using a small scale vibration experiment on a roll of Kapton membrane wound around a mandrel. This experiment demonstrated how the wound roll damper behaves with winding tension. We observed that the addition of the wound roll increased damping observed relative to ‘mandrel-only’ configuration for all winding tensions. The wound roll concept also demonstrated an ability to control the effective stiffness of the assembly where looser winding corresponded to higher damping, but lower stiffness, while tighter winding resulted in decreased

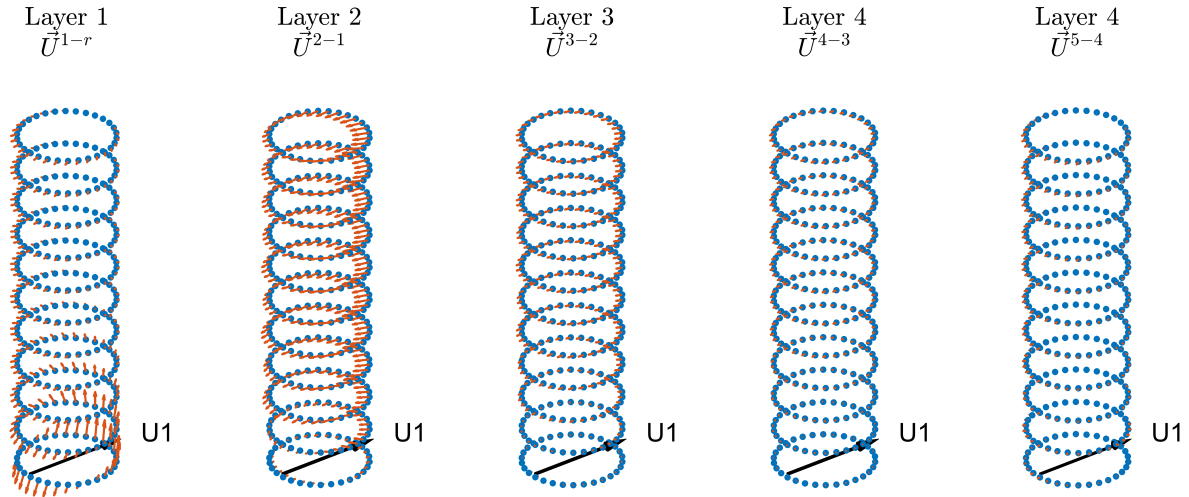


Fig. 14 Maximum relative displacement vectors between adjacent layers for 1g loading.

damping compared to the loosely wound case but with higher stiffness. This suggests a potential tunability of the wound roll damping concept, where stiffness can be traded against damping.

The following slip measurement experiment was able to identify the ‘active’ regions in the wound roll damping concept. These are the regions where slip occurs during vibration and are responsible for the energy dissipation mechanism. High speed camera measurements determined that the vibration mode of the structure dictates the location of the actively slipping regions. For the case of a cantilevered, cylindrical structure with a wound roll damper, subject to base excitation, interlayer slip initiates at the base of the roll from the inner layers. This result indicates that, while the entire coiling form factor plays a role in the stiffness of the assembly, only a limited region may participate in the damping process for a given excitation loading level. This result is salient as it identifies the critical regions for focus when considering techniques to engineer contact properties to control slip for either the purpose of adjusting damping or protecting sensitive surfaces.

The underlying mechanism for the wound roll damper was identified to be the interaction between structure dynamics and interlayer contact properties. This was demonstrated using a relatively simple 3D FEA model, which has shown good, qualitative agreement with experimentally observed damping responses and slip measurements. For a given loading, the locations of maximum shear stresses in the structure are seen at the base, near the mandrel interface. As a result, these are the locations where slip will initiate once the excitation level exceeds the force of friction.

While the FEA model used in this study was able to capture many qualitative behaviors associated with the damping properties of the wound roll damper, there are several quantitative discrepancies that need to be investigated. Specifically, these involve developing a better understanding of the relation between excitation level and friction capacity, in order to achieve closer agreement between simulation and experiment for response amplitudes, damping magnitudes, and response frequencies. Future studies will focus on improving the FEA model to resolve these discrepancies, which will enable this simulation to be used to examine the sensitivity of the wound roll damper to changes in physical parameters, such as the mass and stiffness of the coiled layers, as well as to understand how the damper concept performs at scale.

Acknowledgments

The authors acknowledge financial support from the Space Solar Power Project at Caltech.

References

- [1] Frahm, H., “Device for damping vibrations of bodies, US Pat. No 989,958,” , 1911.
- [2] Fujino, Y., Sun, L., Pacheco, B. M., and Chaiseri, P., “Tuned Liquid Damper (TLD) for Suppressing Horizontal Motion of Structures,” *Journal of Engineering Mechanics*, Vol. 118, No. 10, 1992, pp. 2017–2030. doi:10.1061/(ASCE)0733-9399(1992)118:10(2017).
- [3] Inaudi, J. A., and Kelly, J. M., “Mass Damper Using Friction-Dissipating Devices,” *Journal of Engineering Mechanics*, Vol. 121, No. 1, 1995, pp. 142–149. doi:10.1061/(ASCE)0733-9399(1995)121:1(142).
- [4] Ricciardelli, F., and Vickery, B. J., “Tuned vibration absorbers with dry friction damping,” *Earthquake Engineering & Structural Dynamics*, Vol. 28, No. 7, 1999, pp. 707–723. doi:https://doi.org/10.1002/(SICI)1096-9845(199907)28:7<707::AID-EQE836>3.0.CO;2-C.
- [5] Liu, W., Tomlinson, G., and Rongong, J., “The dynamic characterisation of disk geometry particle dampers,” *Journal of Sound and Vibration*, Vol. 280, No. 3, 2005, pp. 849–861. doi:https://doi.org/10.1016/j.jsv.2003.12.047, URL <https://www.sciencedirect.com/science/article/pii/S0022460X04001282>.
- [6] Okuizumi, N., Mori, O., Matsumoto, J., Saito, K., Sakamoto, H., Torisaka, A., and Shirasawa, Y., “Development of Deployment Structures and Mechanisms of Spinning Large Solar Power Sail,” 4th International Symposium for Solar Sailing, 2017.
- [7] Banik, J., and Hausgen, P., “Roll-Out Solar Arrays (ROSA): Next Generation Flexible Solar Array Technology,” AIAA SPACE and Astronautics Forum and Exposition, 2017. doi:10.2514/6.2017-5307, URL <https://arc.aiaa.org/doi/abs/10.2514/6.2017-5307>.
- [8] Webb, D., Hirsch, B., Bradford, C., Steeves, J., Lisman, D., Shaklan, S., Bach, V., and Thomson, M., “Advances in starshade technology readiness for an exoplanet characterizing science mission in the 2020’s,” *Advances in Optical and Mechanical Technologies for Telescopes and Instrumentation II*, Society of Photo-Optical Instrumentation Engineers (SPIE) Conference Series, Vol. 9912, edited by R. Navarro and J. H. Burge, 2016, p. 99126H. doi:10.1117/12.2232587.
- [9] Wen, A., and Pellegrino, S., “Launch Vibration of Pre-Tensioned Coiled Structures,” AIAA SCITECH 2022 Forum, 2022.
- [10] Umali, J. A., Wilson, L. L., and Pellegrino, S., “Vibration Response of Ultralight Coilable Spacecraft Structures,” 4th AIAA Spacecraft Structures Conference, 2017. doi:10.2514/6.2017-1115, URL <https://arc.aiaa.org/doi/abs/10.2514/6.2017-1115>.
- [11] Torvik, P., “On estimating system damping from frequency response bandwidths,” *Journal of Sound and Vibration - J SOUND VIB*, Vol. 330, 2011, pp. 6088–6097. doi:10.1016/j.jsv.2011.06.027.
- [12] Hartog, *Mechanical Vibrations*, McGraw-Hill, 1947.